Uncertainty quantification and Global Sensitivity Analysis of subsurface flow parameters to gravimetric variations during pumping tests in unconfined aquifers

Fadji Zaouna Maina[1], Alberto Guadagnini[1,2]

[1]Dipartimento di Ingegneria Civile e Ambientale (DICA), Politecnico di Milano, Piazza L. Da Vinci, 32, 20133 Milano, Italy

[2]Department of Hydrology and Atmospheric Sciences, University of Arizona, Tucson, Arizona, USA

Key Points:

- Effect of hydrogeological parameter uncertainty on drawdown, water content and gravity changes during pumping tests in unconfined aquifers
- The strength of the relative contribution of saturated and unsaturated zone parameters to gravimetric variations markedly varies over time
- Gravimetric information are mostly sensitive to specific yield and aquifer specific storage, especially at early pumping times

Abstract

We study the contribution of typically uncertain subsurface flow parameters to gravity changes that can be recorded during pumping tests in unconfined aquifers. We do so in the framework of a Global Sensitivity Analysis and quantify the effects of uncertainty of such parameters on the first four statistical moments of the probability distribution of gravimetric variations induced by the operation of the well. System parameters are grouped into two main categories, respectively governing groundwater flow in the unsaturated and saturated portions of the domain. We ground our work on the three-dimensional analytical model proposed by Mishra and Neuman (2011), which fully takes into account the richness of the physical process taking place across the unsaturated and saturated zones and storage effects in a finite radius pumping well. The relative influence of model parameter uncertainties on drawdown, moisture content and gravity changes are quantified through (*a*) recently developed indices quantifying the relative contribution of each uncertain model parameter to the (ensemble) mean, skewness and kurtosis of the model output, and (*b*) the Sobol' indices, derived from a classical decomposition of variance. Our results document (*i*) the importance of the effects of the parameters governing the unsaturated flow dynamics on the mean and variance of local drawdown and gravity changes; (*ii*) the marked sensitivity (as expressed in terms of the statistical moments analyzed) of gravity changes to the employed water retention curve model parameter, specific yield and storage, and (*iii*) the influential role of hydraulic conductivity of the unsaturated and saturated zones to the skewness and kurtosis of gravimetric variation distributions. The observed temporal dynamics of the strength of the relative contribution of system parameters to gravimetric variations suggest that gravity data have a clear potential to provide useful information for estimating the key hydraulic parameters of the system.

1. Introduction

Pumping tests are typically designed and implemented to enhance our ability to characterize aquifer systems. They provide valuable information about hydrodynamic parameters (e.g., permeability and/or storage) through the analysis of the system response. The latter is usually considered in terms of drawdown, which represents the variation of hydraulic head at a given point due to pumping. Analytical solutions as well as numerical methods have been proposed by several authors to describe and interpret pumping test responses to improve hydrogeological description of a tested system. These include, e.g., the works of Theis (1935), Hantush (1964), Neuman (1972, 1974), Moench (1997a), Raghavan, (2004), Tartakovsky and Neuman (2007), Moench (2008), Mishra and Neuman (2010). In this context, it is recognized that characterizing aquifer parameters by constraints associated with pumping test data is not obvious or trivial. For example, it is known that under some conditions, storage and hydraulic conductivity (or transmissivity) can be estimated through pumping responses at short and long times, respectively. Depending on the pumping rate and aquifer hydrogeological setting, the extent of time period within which pumping test data can provide useful information to assess storage can be remarkably variable, thus hampering our ability to optimize the design of a pumping test to fully exploit the information content encapsulated in drawdown data.

In this context, estimation of hydrological parameters can benefit from the joint use of hydrological and geophysical information. Geophysical investigations are typically non-invasive and can provide information associated with a large volume of the aquifer system under investigation. Methods which are commonly employed include ground-penetrating radar (Bevan et al., 2003), self-potential responses (Rizzo et al., 2004; Straface et al., 2007), or electrical resistivity imaging (Chang et al., 2017.). Among the sets of geophysical data which can be of interest, gravimetric measurements are increasingly considered to carry valuable information to effectively complement drawdown data for aquifer characterization. Monitored gravity variations have been shown to embed a remarkable information content and are employed in several applications, including, e.g., geothermal energy (Hunt, 1977; Hunt and Bowyer, 2007; Hunt and Graham, 2009; Sofyan et al., 2011; Hinderer et al., 2015) or petroleum engineering (Alnes et al., 2008; Eiken et al., 2008; Young and Lumley, 2015; Kabirzadeh et al., 2017; Katterbauer et al., 2017). Local variations in the acceleration of gravity are due to the Newtonian attraction and to deformations created by loads/stresses. As such, they are linked to a variety of causes, including variations of loading due to displacement of masses of water, as in the cases of, e.g., oceans and atmospheric masses or displacement of fluids in the subsurface. In the context of subsurface hydrology, gravity changes of the order of several μGal have been documented (Damiata and Lee, 2006; Jacob et al., 2008a). These can be detected by modern gravimeters, which can have a resolution of the order of the μGal (corresponding to about 5cm of water table variation (Jacob et al., 2008a)). Absolute gravimeters are widely used in hydrology and have the advantage of being (*a*) readily transported and (*b*) non-invasive, so that one can measure variations of gravity at several points in space.

The study of Montgomery (1971) is considered as one of the first documented applications of gravimetric data to a hydrological setting, its main target being the estimation of storage of a sandy aquifer in Arizona. Since then, the use of the technique in hydrology applications has gained popularity. Notable examples include the large scale study GRACE (Gravity Recovery and Climate Experiment), where data provide improved understanding of water mass variations with a resolution of about 500 km (Tapley et al., 2004; Andersen and Hinderer, 2005; Andersen et al., 2005). Gravity data have also been used for (*a*) the characterization of aquifers located in arid regions (Andersen and Hinderer, 2005; Hinderer et al., 2009; Pfeffer et al., 2011); (*b*) the study of aquifer recharge, eventually in the context of injection tests (Hunt, 1977; Pool, 2005, 2008; Gehman et al., 2009); (*c*) the characterization of karstic aquifers (Jacob et al., 2008b, 2009, 2010; Wilson et al., 2012); and (*d*) the estimation of hydrodynamic parameters (Pool and Eychaner, 1995; Naujoks et al., 2010; Christiansen et al., 2011).

A few recent studies are focused on the analysis of the variation of gravity which could be observed during pumping tests in unconfined aquifers. Damiata and Lee (2006) show that gravimeters have the potential of detecting the effects of variations in hydraulic heads caused by a pumping well and rendering estimates of hydrodynamic parameters. Blainey et al. (2007) show that our ability to estimate hydrodynamic parameters of an aquifer is enhanced through a joint use of direct drawdown and gravimetric data. These two preliminary works are limited to fully penetrated wells operating in homogeneous and isotropic aquifers. Herckenrath et al. (2012) extend the results of these studies by considering aquifers with anisotropic conductivity where partially penetrating wells are operating. These authors based their analysis on the analytical solution of Moench (1997b), which is employed to describe head drawdown. This analytical solution does not explicitly take into account effects due to (*a*) the presence of an unsaturated region that might overlay the groundwater table prior to pumping, and (*b*) the system dynamics in the portion of the aquifer which is subject to dewatering during pumping, the rate of drainage from the unsaturated zone being modeled as a boundary condition at the water table.

Our work is specifically targeted to the analysis of the gravity changes that can be observed during a pumping test in an unconfined aquifer. Due to the importance of the impact of the unsaturated zone on head drawdowns documented by detailed field experiments (Bevan et al., 2003), numerical studies based on analytical solutions (Mishra and Neuman, 2011) or numerical analyses (Delay et al., 2012), we ground our study on the very recent three-dimensional analytical solution proposed by Mishra and Neuman (2011). The latter fully takes into account the effects of the flow dynamics across the unsaturated and saturated zones and the features of the pumping well, which is characterized by a finite radius and storage. Gravity changes induced by the drawdown caused by pumping are quantified through the method proposed by Leirião et al. (2009).

Starting from the recognition that model parameters are typically uncertain, the distinctive aim of our study is the assessment of the sensitivity of the hydrodynamic model parameters of the groundwater system to (*a*) local drawdown, (*b*) variation of moisture content, and ultimately (*c*) gravity changes induced by pumping. In this context, model parameters can be conceptualized as random variables, and their uncertainty can then propagate to target model outputs. As such, the analyses we illustrate contribute to assess the relative importance of uncertain model parameters on statistical moments of the model output of interest. They are also conducive to the assessment of the degree of information content embedded in hydrological and gravimetric information of the type we consider.

While previous studies have concluded that some of these parameters can be identified using gravimetric variations, no study has considered a complete solution of the flow scenario of the kind we analyze. Blainey et al. (2007) study the contributions of gravity measurements to hydraulic parameter estimation and performed local sensitivity analyses for a given virtual setup. Herckenrath et al. (2012) analyze the effect of coupling magnetic resonance sounding and gravity data monitored during a pumping test for the identification of aquifer parameters through inverse modeling. These studies are based on the model developed by Moench Barlow and Moench (1999) and Moench, (1996, 1997). As such, the assessment of hydrodynamic parameter identifiability was only limited to saturated hydraulic conductivity and specific yield.

Our study differs from previous works in terms of (*i*) the richness of the physical processes included in the analytical model employed and (*ii*) the type of sensitivity analysis we perform. With reference to the latter aspect, we frame our study in the context of a Global Sensitivity Analysis (GSA) approach, recent studies and reviews on this methodology being illustrated by, e.g., Pianosi and Wagener (2015) Razavi and Gupta, (2015) Sarrazin et al. (2016). Our GSA is then complemented by the quantification of the way the uncertainty of model parameters propagates to model outputs, i.e., temporal dynamics of local drawdown and moisture content as well as gravity changes. We aim at answering the following research questions: which model parameters are most influential to drawdown, moisture content and (local and/or global) gravity changes? At which times? We answer these questions by grounding our GSA on the recent work of Dell'Oca et al. (2017), who propose a set of indices that quantify the relative contribution of each uncertain model parameter to the (ensemble) mean, skewness and kurtosis of the model output, and on the Sobol' indices (e.g., Sobol, (1993)), derived from a classical decomposition of variance.

The work is organized according to the following structure. Section 2 recalls the main assumption underlying the flow model we rely upon and the link between drawdown and gravity changes in the unsaturated and saturated zone. Section 3 illustrates briefly the GSA we perform and the associated indices. Our results are discussed in Section 4, where we quantify the contribution of the uncertainty associated with each model parameter to the average and variance of drawdown, moisture content and gravity changes during a pumping test.

2. Theoretical framework

2.1 Groundwater table drawdown during a pumping test

We describe drawdown in an unconfined aquifer subject to pumping by way of the recent analytical solution developed by Mishra and Neuman (2011). The latter considers a partially penetrating well and takes into account the presence of an unsaturated zone initially located above the water table as well as the dynamics of flow within the portion of the aquifer that is de-saturated during pumping.

A compressible aquifer of infinite lateral extent is considered. The aquifer is assumed to be homogeneous and anisotropic, K_r and K_z respectively denoting horizontal and vertical saturated hydraulic conductivities. The water table is initially located at elevation $z = b$. Pressure head ψ at the water table corresponds to atmospheric pressure, i.e., $\psi = \psi_a$, and is typically set to 0.0. The initial thickness of the unsaturated zone is denoted as *L*, ground surface being located at elevation $z = b + L$. A sketch of the system geometry is depicted in Figure 1. Hydraulic head in the unsaturated zone is initially uniform and equal to $h_0 = b + \psi_a$. A pumping well penetrates the aquifer and is screened between elevations *l* and *d* (see Figure 1). The pumping rate *Q* at which the well is operated is uniform in time. The equation describing the water movement in the saturated zone can then be written in cylindrical coordinates as:

$$S_s \frac{\partial s}{\partial t} = K_r \frac{1}{r}\frac{\partial}{\partial r}\left(r \frac{\partial s}{\partial r} \right) + K_z \frac{\partial^2 s}{\partial z^2} \tag{1}$$

S_s being specific storage. Drawdown *s* is given by

$$s(r,z,t) = h(r,z,0) - h(r,z,t) \tag{2}$$

h being hydraulic head at elevation *z*, time *t* and radial distance *r* from the well.

The initial and boundary conditions associated with (1) are

$$\begin{aligned}
& s(\infty, z, t) = 0 \\
& \frac{\partial s}{\partial z} = 0 \quad z=0 \\
& \lim_{r \to 0} r \frac{\partial s}{\partial r} = 0 \quad 0 \le z \le b - l \qquad b - d \le z \le b \\
& \lim_{r \to 0} r \frac{\partial s}{\partial r} = -\frac{Q}{2\pi K_r (l - d)} \quad b - l \le z \le b - d
\end{aligned} \tag{3}$$

Flow in the unsaturated zone is described by the Richards' equation (Richards, 1931), i.e., following Tartakovsky and Neuman (2007).

$$C_0(z)\frac{\partial \sigma}{\partial t} = K_r k_0(z)\frac{1}{r}\frac{\partial}{\partial r}\left(r\frac{\partial \sigma}{\partial r}\right) + K_z\frac{\partial}{\partial z}\left(k_0(z)\frac{\partial \sigma}{\partial z}\right) \qquad b < z < b+L \tag{4}$$

Here, σ is drawdown in the unsaturated zone, given by

$$\sigma(r,z,t) = h_0 - h(r,z,t) = b + \psi_a - h(r,z,t) \tag{5}$$

$C_0(z)$ is the specific moisture capacity defined as $C_0(z) = C(\theta_0)$ (θ being water content, the subscript 0 indicating the initial conditions), and $k_0(z)$ the relative hydraulic conductivity. Note that both $C_0(z)$ and $k_0(z)$ are not depending on the radial distance from the well.

Equation (3) is complemented by the following initial and boundary conditions

$$\begin{aligned} &\sigma(\infty,z,t) = 0 \\ &\frac{\partial \sigma}{\partial z} = 0 \quad z = b+L \\ &\lim_{r\to 0} r\frac{\partial \sigma}{\partial r} = 0 \quad b \le z \le b+L \end{aligned} \tag{6}$$

The aquifer water retention curve is represented as (see Mishra and Neuman (2011))

$$S_e = \frac{\theta(\psi) - \theta_r}{S_Y} = e^{a_c(\psi - \psi_a)} \qquad a_c \ge 0 \tag{7}$$

where a_c is a model parameter, $\theta(\psi)$ is water content, S_e is effective saturation, $S_Y = \theta_s - \theta_r$ is specific yield, and θ_s and θ_r respectively are water content at saturation and residual water content.

The Gardner exponential model (Gardner et al., 1958) is used to characterize relative hydraulic conductivity, i.e.,

$$k(\psi) = \begin{cases} e^{a_k(\psi - \psi_k)} & \psi \le \psi_k \\ 1 & \psi < \psi_k \end{cases} \qquad a_k \ge 0 \tag{8}$$

$a_k \neq a_c$ and $\psi_k \neq \psi_c$ being model parameters. The parameter $\psi_k \leq 0$ is usually the air entry pressure head and represents the pressure head above which $k(\psi)$ is effectively equal to unity.

Coupling of the flow across saturated and unsaturated zones is achieved by assuming that pressure is continuous at and flux is normal through the water table. Equations (1) and (4) are thus coupled by way of

$$\begin{aligned} s - \sigma = 0 \qquad z = b \\ \frac{\partial s}{\partial z} - \frac{\partial \sigma}{\partial z} = 0 \qquad z = b \end{aligned} \tag{9}$$

Mishra and Neuman (2010) write the drawdown in the saturated zone as

$$s = s_H + s_U \tag{10}$$

Here, s_U is the component of the drawdown accounting for the contribution of the unsaturated zone on the water table fluctuation; and s_H is a modified Hantush solution (Hantush, 1964). Whereas the Hantush solution describes flow towards a partially penetrating well of zero radius in a confined aquifer, the modified solution introduced by Mishra and Neuman (2011) accounts for storage effects in a partially penetrating pumping well with finite radius r_w and storage coefficient C_w.

2.2 Gravity variations due to groundwater table drawdown

Gravimetric variations within a time interval δt are due to change in the water content, expressed in terms of mass, in the domain. Considering a cylindrical coordinate system, the following formulation can be employed to quantify such variations, as detected by a gravimeter located at (r_m, z_m) within a domain of infinite extent (Telford et al., 1990)

$$\Delta g = \int_{-\infty}^{+\infty} \int_{-\infty}^{+\infty} \gamma \Delta\rho(r,z) \frac{-(z - z_m)}{\left((r - r_m)^2 + (z - z_m)^2\right)^{3/2}} \, dz dr \tag{11}$$

Here, Δg (L T^{-2}) is the variation of gravity (or gravity change) between time t from the beginning of pumping and the initial (undisturbed) conditions and caused by a change of mass at locations associated with radial coordinate r and vertical coordinate z where a density change $\Delta\rho$ (M L^{-3}) takes place, and γ = 6.67 × 10^{-11} (N m^2 kg^{-2}) is the universal gravitational constant.

Density changes $\Delta\rho$ within a volume $\Delta\Omega = \left(\pi\left(r+dr\right)^2 - \pi r^2\right)dz$ depend on the change of (*a*) water head, Δh, in the saturated zone and (*b*) water content, $\Delta\theta$, in the unsaturated region through

$$\Delta\rho = \rho_w S_s \Delta h \tag{12}$$

$$\Delta\rho = \rho_w \Delta\theta \tag{13}$$

where $\Delta\theta$ can be evaluated via (7) and ρ_w is water density, (12) and (13) respectively referring to the saturated and unsaturated regions. The global change in gravity at the scale of the pumping test is then obtained by the numerical integration of (11).

3. Global Sensitivity Analysis

As highlighted by (11) - (13), gravity changes depend on a set of hydrogeological parameters. The uncertainty associated with these parameters is typically due to lack of information and is then propagated to state variables of interest, notably to Δg, Δh, and local moisture content or effective saturation. Global Sensitivity Analysis (GSA) provides a theoretical framework within which one can then quantify the influence of these uncertain quantities on key (statistical) moments of target model output quantities. In this context, we focus on four sets of indices: (*i*) the indices introduced by Dell'Oca et al. (2017), and (*ii*) the Sobol' indices (Sobol, 1993). These indices respectively enable us to quantify the relative contribution of each uncertain model parameter to the mean (expected value), variance, skewness, and kurtosis of the state variable of interest. Having at our disposal this information enables us to rank model parameters in order of importance with respect to a given statistical moment of the model output.

Performing a GSA requires spanning the entire parameter space and performing multiple runs of the process model of choice in a Monte Carlo framework. In some cases, this might lead to high computational costs, which can hamper the practical feasibility of the analysis. It has then become common procedure to approximate the complete system model through a surrogate model. The latter can be considered as a reduced complexity approximation of the original model and can be employed to perform multiple Monte Carlo runs with a sufficient accuracy and at an affordable computational time. As noted by Mishra and Neuman (2010, their Appendix C and D), the analytical solution we employ can be computationally demanding. For example, we verified that calculation of the solution at one point for the full simulation time can take up to 1 hour to 20 hours on a computer Intel Core i7 3.20GHz, depending on the parameter set values, due to the need for evaluating numerous integrals. As a consequence, we resort to a strategy based on the construction of a surrogate model to perform GSA in our study. Amongst available alternatives, we base our GSA on the formulation of a surrogate model based on the Polynomial Chaos Expansion (PCE) framework. The latter has been broadly used to perform GSA in various fields of applications (Sudret, 2008; Crestaux et al., 2009; Fajraoui et al., 2011; Formaggia et al., 2012; Ciriello et al., 2013a; Fajraoui, 2014; Garcia-Cabrejo and Valocchi, 2014; Sudret and Mai, 2015) and yields the target global sensitivity indices in a straightforward manner.

We briefly summarize in the following the theoretical elements characterizing the GSA indices we employ and the PCE technique. We refer to appropriate literature for additional details.

3.1. The AMA indices (Dell'Oca et al., 2017)

As observed by Dell'Oca et al. (2017), a limitation of grounding a GSA solely on the Sobol' indices (see also Section 3.2 for a synthetic illustration of these indices) is that the uncertainty of a target model output, *y*, is considered to be fully characterized by its variance. As such, ranking the relative importance of model parameters upon relying solely on the analysis of Sobol' indices might provide an incomplete picture of a system response to model parameters. Here, we also quantify the effects that uncertain model parameters can have on the mean (expected value) of *y*, to broaden the scope of the GSA we perform. We do so by relying on the metrics introduced by Dell'Oca et al. (2017), i.e.,

$$AMAE_{x_i} = \frac{1}{|y_0|}\int_{\Gamma_{x_i}} \left|y_0 - E[y \mid x_i]\right| \rho_{\Gamma x_i} dx_i = \frac{1}{|y_0|} E\left[\left|y_0 - E[y \mid x_i]\right|\right] \tag{14a}$$

$$AMA\gamma_{x_i} = \frac{1}{\left|\gamma\left[y\right]\right|}\int_{\Gamma_{x_i}} \left|\gamma\left[y\right] - \gamma[y \mid x_i]\right| \rho_{\Gamma x_i} dx_i = \frac{1}{\left|\gamma\left[y\right]\right|} E\left[\left|\gamma_y - \gamma[y \mid x_i]\right|\right] \tag{14b}$$

$$AMAk_{x_i} = \frac{1}{k\left[y\right]}\int_{\Gamma_{x_i}} \left|k\left[y\right] - k[y \mid x_i]\right| \rho_{\Gamma x_i} dx_i = \frac{1}{k\left[y\right]} E\left[\left|k\left[y\right] - k\left[y \mid x_i\right]\right|\right] \tag{14c}$$

Here, y_0, $\gamma\left[y\right]$, and $k\left[y\right]$ respectively are the mean, skewness and kurtosis of *y*, $\Gamma_{x_i} = [x_{i,\min}, x_{i,\max}]$ is the support of the *i*-th random variable x_i (ranging between $x_{i,\min}$, and $x_{i,\max}$; $E\left[y \middle| x_i\right]$, $\gamma[y \mid x_i]$, and $k\left[y \mid x_i\right]$ respectively are the mean, skewness, and kurtosis of *y* conditional on x_i; and $\rho_{\Gamma_{x_i}}$ is the marginal probability density function (*pdf*) of x_i. Similar to the Sobol' indices, we can also evaluate the joint effect of parameters on the mean and therefore the total index associated with a given parameter. Evaluation of the indices (14a)-(14c) enables us to quantify the expected variation of the corresponding statistical moments of a target quantity due to conditioning on a given system parameter. Relying on these indices provides information on the way features of the probability distribution of *y* (i.e., mean, symmetry, and tailedness) can be influenced by uncertain model parameters. The reader is referred to Dell'Oca et al. (2017) for additional details.

3.2. The Sobol' indices

Let us consider the output y of a mathematical model f having n input parameters $\left(x_1, x_2, ..., x_n\right)$, i.e.,

$$y = f\left(x_1, x_2, ..., x_n\right) \tag{14}$$

We assume f to belong to the space of square integrable functions and the n uncertain input parameters to be defined in $\left[0,1\right]^n$. The function f can be decomposed into sums of polynomials of increasing power, i.e.,

$$f\left(x_1, x_2, ..., x_n\right) = f_0 + \sum_{i=1}^{n} f_i\left(x_i\right) + \sum_{j>1}^{n} f_{ij}\left(x_i, x_j\right) + ... + f_{1,2,...,n}\left(x_1, x_2, ..., x_n\right) \tag{15}$$

where f_0 is the expected value of f, and $f_{1,2,...,n}\left(x_1, x_2, ..., x_n\right)$ are orthogonal functions.

Decomposition (16) is based on the analysis of variance (ANOVA, Archer et al., 1997) and is unique. By squaring (16) and integrating over $\left[0,1\right]^n$, we obtain

$$V = \sum_{i=1}^{n} V_i + \sum_{j>1}^{n} V_{ij} + ... + V_{1,....,n} \tag{16}$$

Here, V is the total variance of y, V_i and V_{ij} respectively being the contribution to V due to input x_i alone and due to the interactions of parameters x_i and x_j.

The principal Sobol' sensitivity indices (Sobol, 1993) are given by

$$S_i = \frac{V_i}{V} \tag{17}$$

and describe the relative contribution to V due to variability of only x_i. Note that the principal Sobol' index embeds the relative expected reduction of the variance of y due to knowledge of (or conditioning on) parameter x_i.

Otherwise, the total Sobol' indices

$$S_i^{tot} = \frac{\sum_{i\in\{i_1,....,i_s\}} V_{i_1,....,i_s}}{V} \tag{18}$$

quantify the total contribution of x_i to V, including all terms where x_i appears, i.e., S_i^{tot} also includes interactions between x_i and the remaining uncertain parameters.

3.3. Construction of the surrogate model using polynomial chaos expansion

Relying jointly on the AMAE (14a), AMAγ (14b), AMAk (14c), and Sobol' indices (introduced in Sections 3.2.1 and 3.2.2) enables one to perform a GSA of process *y* quantifying the impact of each of the uncertain model parameters on the first four (statistical) moments of the *pdf* of *y*. This strategy yields information about the way these important elements of the distribution of *y* are impacted by model uncertain parameters. Calculation of these indices entails evaluation of conditional moments of *y* that are here computed using the PCE - based approximation of the full system model.

Following Wiener (1938) and Xiu and Karniadakis (2002), we represent $f(\boldsymbol{x})$ ($\boldsymbol{x}$ being the vector collecting random system parameters x_i, i =1, 2, ..., n) as

$$f(x) = \sum_{j=0}^{+\infty} a_j \zeta_j (x_1,......,x_n) \tag{19}$$

where a_j are polynomial coefficients and $\zeta_j(x_1,......,x_n)$ are multivariate orthogonal polynomials which depend on the joint probability function of the random model parameter. For computational purposes, decomposition (19) is truncated to a finite order *M* as

$$y = a_0\xi_0 + \sum_{j=1}^{M-1} a_j \xi_1\left(x_j\right) + \sum_{j \geq i}^{M-1} a_{ij} \xi_2\left(x_j, x_i\right) + \sum_{k \geq j}^{M-1} a_{ijk} \xi_3\left(x_j, x_i, x_k\right) + \dots\dots\dots \quad (20)$$

where $M = \dfrac{(n+p)!}{n!\,p!}$, p being the polynomial degree retained for each function ξ_i.

Coefficients a_j are calculated through an approach that requires evaluating the full system model at a number of points in the parameter space and then performing least square regressions (Sudret, 2008). We note that the number of coefficients may be prohibitively large when the number of random model parameters increases. Thus, several approaches have been developed to minimize computational cost by appropriate selection of model evaluation points in the parameter space (e.g., Blatman and Sudret, 2010b, 2010a, 2011; Fajraoui et al., 2012) and reference therein. Here, we apply the sparse grid sampling technique suggested by Fajraoui et al. (2012). Following this approach, only coefficients whose contribution to the output is higher than a user defined threshold are retained, thus reducing the number of full model simulations required to estimate the polynomial coefficients. Sobol' indices are evaluated as the coefficients of the PCE, the AMAE, AMAγ, and AMAk indices being computed through Monte Carlo runs of the PCE.

4. Sensitivity of drawdowns, effective saturation and gravity changes to hydrogeological parameters during a pumping test

4.1 Problem set-up

We consider an unconfined homogeneous aquifer whose water table is located 10 m below the ground surface and the initial hydraulic head is equal to 50 m. A partially penetrating pumping well is operating in the system. In our example, the well is screened from 39 m to 40 m below the ground surface and is operated at a uniform pumping rate Q = 6.30×10^{-2} m^3/s. The well is characterized by a dimensionless radius r_{wD} = r_w/b = 0.02 and storage $C_{wD} = C_w/b = 0.10$. A gravimeter is installed on the surface and at the same position as the pumping well (Figure 1).

Drawdowns are computed at a set of radial distances, defined according to a logarithmic spacing, i.e.,

$$\begin{aligned} r_1 &= \Delta r \\ r_i &= 10^{\log(r_{i-1})+\Delta r} \end{aligned} \tag{21}$$

where Δr = 10 m. At each radial distance, drawdown is also computed along the vertical at a set of elevations arranged according the same logarithmic spacing design as in (21).

We simulate the test across 7 days of operation. This duration is consistent with duration of pumping tests in unconfined systems (see, e.g., Bevan et al. (2003) and references therein) and allowed to reach pseudo-steady state for the mean drawdown in our study. We also note that the scenario analyzed corresponds to the one presented by Darmiata and Lee (2006) and Leiriao et al. (2009) and can then be considered as a proxy for a field scale test, in terms of positioning and flow rate of the well, duration of the pumping operation, and range of variability of the system parameters. We perform a GSA of the drawdown, soil moisture and gravimetric variations to the following dimensionless parameters: (*a*) $\mathrm{L}_D = L/b$, which is a characteristic (dimensionless) system length scale; (*b*) the anisotropy factor $\mathrm{K}_D = K_z / K_r$; (*c*) the specific storage of the saturated zone S_S; (*d*) the specific yield S_Y, (*e*) $a_{cD} = a_c b$ and $a_{kD} = a_k b$, which are respectively associated with the parameters used in the water retention and relative hydraulic conductivity functions.

Model uncertain parameters are considered as independent and identically distributed (*i.i.d.*) random variables, each characterized by a uniform distribution within the intervals listed in Table 1. These intervals are normalized between (0, 1) for the construction of the PCE. We perform 500 full model simulations within a Quasi Monte Carlo sampling approach, a sampling technique that has desirable convergence properties and is space filling (Feil, 2009). PCE models of increasing order were built by considering 400 simulations, randomly selected amongst the total number of simulations performed. The accuracy of the ensuing PCE for drawdowns, soil moisture and gravity changes were evaluated by cross-validations against the remaining 100 simulations. The procedure was repeated by considering various sets of randomly selected simulations for the construction and validation of the PCE. A PCE of order 4 was considered as appropriate in terms of accuracy (details not shown).

4.2. Results and discussion

We present our results at two scales, i.e., a small scale, representing a volume of the aquifer that can be considered as the measurement scale of heads and moisture content and the global scale of the pumping test, which represents the scale at which pointwise gravity changes are integrated by the gravimeter.

4.2.1 Temporal variations of drawdown, effective saturation and gravity changes at a local scale

We illustrate here the analyses of the sensitivity of our target variables to the selected uncertain model parameters at a local scale. We define the latter as a volume of size $V=\left[\pi\left(r+\Delta r/2\right)^2-\pi\left(r-\Delta r/2\right)^2\right]\Delta z$ with $\Delta r=\Delta z=10\,\mathrm{m}$, centered at a given point *A* in the aquifer. For purpose of illustration, we position *A* at the initial position of the interface between the saturated and the unsaturated zones (i.e., r = z = 10 m). This location has been chosen since it is close to the well and enables us to clearly highlight the diverse contributions of parameter uncertainty to the variables of interest, i.e., drawdown, effective saturation and gravity changes.

Figure 2a depicts the temporal evolution of the mean (continuous curve) drawdown and its related uncertainty at this location based on 500 runs of the analytical solution. The level of uncertainty is illustrated by the shaded area whose limits correspond to one standard deviation. A corresponding depiction of the temporal dynamics of effective saturation is shown in Figure 2b.

The observed evolution of the mean drawdown imbues the effects of an artesian storage during early times (until about 3000 s from the beginning of pumping) and drainage from the unsaturated zone during late times.

The effective saturation, S_e, can also be directly measured in the field and represents the variations of the water content in the unsaturated zone. As expected, the mean effective saturation of the considered volume decreases with time. It is noted that there is a very significant impact of the parameter uncertainty, as quantified by the variance of S_e.

The corresponding temporal dynamics of gravity changes detected between the initial (undisturbed) condition and time *t* are due to the temporal variation of mass of water in the volume considered and are depicted in Figure 3. Note that here and in the following we denote gravity change calculated at time *t* as the difference between gravity at *t* and at the initial system state. These changes range on average between 0.0 and 0.5 μGal, and can attain values as large as 2 μGal at late times. We note that, as stated above, these results are associated with a local scale volume that is in the vicinity of the well and of the ground surface, where the gravimeter is positioned, so that the drawdown taking place within it markedly contributes to the gravity change detected by the gravimeter. Comparison of Figures 2 and 3 suggests that the variance of gravity changes, Δg, is larger and increases at a higher temporal rate than that of drawdown, Δh. This is related to the structure of (11)-(13), from which it can be seen that a random gravity change is proportional to the product of two (correlated) random quantities, i.e., S_S and Δh in (12) or $\Delta \theta$ in (13) the latter, in turn, depending on S_Y, Δh and a_{cD}.

Figure 4 depicts the contribution of the uncertainty of each model parameter to the mean (i.e., in terms of AMAE indices (14a) in Figure 4a) and to the variance (i.e., in terms of

Sobol' indices in Figure 4b) of drawdown. These results show that the specific storage S_S is the main parameter governing the mean and variance of drawdown during the first hours of pumping (up to approximately 3,000 s). The uncertainty related to the anisotropic factor K_D has an essentially uniform contribution to the average drawdown (Figure 4a) after 30,000 s; it contributes significantly to drawdown variance (Figure 4b) between time t = 3,000 s and 100,000 s, as compared to the parameters related to the unsaturated zone (i.e., S_Y, a_{kD}, and a_{cD}). Contributions of the parameters characterizing the unsaturated zone appear to be non-negligible only at late times, when the contribution of the parameters related to the saturated zone becomes of secondary importance.

The sensitivity of the drawdown to the unsaturated zone parameters tend to increase with time, while the contribution of the specific storage is observed to acquire lesser importance. This is due to the effects of artesian storage taking place during early pumping times. It can be observed that the sensitivity of the specific storage to the mean drawdown starts decreasing as soon as pumping starts (Figure 4a), its sensitivity to drawdown variance remaining constant during the first minutes of pumping (Figure 4b). The mean and variance of the drawdown are insensitive to the initial thickness of the unsaturated zone, L_D. This is consistent with the conclusions of Mishra and Neuman (2011), who pointed out that the initial unsaturated zone thickness (when greater than one quarter of the saturated thickness) has no significant effect on the drawdown. The drawdown in the saturated zone depends solely on the unsaturated flow dynamics taking place close to the water table.

The parameters used to model flow in the unsaturated zone, a_{cD} and a_{kD}, attain the highest importance for the longest observation times, corresponding to the drainage of the unsaturated zone. At late pumping times, the most significant contributions to the mean and variance of drawdown are due to the uncertainty related to a_{cD} and a_{kD}. Hydraulic conductivity of the unsaturated zone decreases rapidly with pressure for high values of a_{kD} (see (8)), thus causing an increase of the drawdown in the saturated zone, because the unsaturated zone provides less water. Very large values of a_{kD} lead to a virtually impermeable unsaturated zone. The unsaturated zone loses its ability to store water above the water table also for large values of a_{cD}, causing an increase of the contribution of the unsaturated zone to the drawdown (drainage) and therefore, the drawdown decreases at the beginning of the pumping test. The capacity of the unsaturated zone to store water increases when a_{cD} is small, this scenario causing delayed water table response and drawdown at the beginning of the pumping test.

Figure 5 depicts the temporal evolution of both sets of GSA indices evaluated for effective saturation S_e within the same sample volume corresponding to Figure 4. The water retention parameter a_{cD} contributes in very distinct ways to the mean (Figure 5a) or to the variance (Figure 5b) of the effective saturation, i.e., its contribution increasing or being approximately uniform in time for the mean and for the variance. The high sensitivity of a_{cD} is consistent with the observation that it quantifies the amount of water released for a given pressure drop (see (7)). The opposite behavior is documented for the specific storage S_S, whose contribution remains constant for the mean and decreases with time for the variance. Similar to the drawdown, the effective saturation is sensitive to S_S solely during the early time of pumping.

Variability in gravity changes are mainly controlled by the specific yield S_Y, the specific storage S_S, and the water retention curve parameter a_{cD} (Figure 6). The relative contribution of conductivity anisotropy and unsaturated zone parameters (L_D and a_{kD}) to the mean gravity changes is significant. This is clearly seen in Figure 6a, where these parameters are seen to be associated with sensitivity indices which are almost constant with time and greater than 0.25. The influences on the variance of the gravity changes (Figure 6b) of the parameters are negligible (with total Sobol' indices less than 0.05) except for the parameters related to water storage (i.e., specific yield and specific storage) and a_{cD}. Unlike the drawdown, we found that the mean gravity changes are slightly sensitive to the initial thickness of the unsaturated zone. Gravity changes depend on drawdown, distance from the gravimeter, the specific yield and the parameter a_{cD} associated with the dynamics of the unsaturated zone, as well as on the specific storage of the saturated zone. Therefore, gravity changes due to pressure head variations in the saturated zone are significantly smaller than those due to pressure head variations in unsaturated zone.

4.2.2 Total gravity changes at the pumping test scale

The gravimeter yields a measure of the gravity changes occurring throughout the whole region affected by pumping. Note that, according to (11), the contribution of a given point in the aquifer (that can be considered as the centroid of a given measurement volume of the kind explored, e.g., in Section 4.2.1) is weighted by the square of its inverse distance from the gravimeter. Figure 7 depicts the evolution with time of the mean gravity change detected over the whole domain (Figure 7a) and of the sample probability density functions of gravity changes (Figure 7b) associated with three selected observation times (i.e., 100 s, 4 h, and 7 days). These results show that the mean and variance of the global variations of gravity at the scale of the pumping test display a trend which is similar to that observed at the local scale (compare Figures 7 and 3). The largest mean value is approximately equal to 1.14 μGal and is obviously attained at the end of the pumping period, where a quite large variance is also observed (the variance is equal to 1.3 $\mu\mathrm{Gal}^2$, the associated coefficient of variation being 1). The resulting sample probability density function at a given observation time can be interpreted through an Exponential distribution, as shown in Figure 7b, the corresponding scale parameter coinciding with the mean value depicted in Figure 7a. Close inspection of the sample probability densities depicted in Figure 7 reveals that in some regions of the parameter space gravity changes at late time (i.e., 7 days) can be significant. For example, they can attain values as large as 5 or 6 μGal with non-negligible probability. Otherwise, probability that total gravity changes be larger than, e.g., 5 μGal is virtually negligible for all practical purposes at early time. These results suggest that, depending on the characteristic system parameters, there is a clear potential to discriminate total gravity changes due to the effect of pumping at late time with typical instrumentations. The latter can be associated with sensitivities and accuracy which are compatible with the gravity change values we find, depending on conditions (e.g, Merlet et al., 2008; Jacob et al., 2009; Gehman et al., 2009; Christiansen et al., 2011a, b; González-Quirós and Fernández-Álvarez, 2017). As an additional comment, we note that in this study we assess total gravity changes measured across the pumping test through a single gravimeter located at the well position. A possible extension of the analysis would entail the use of a network of gravimeters, arranged according to a given pattern. This would be associated with the added value of enhancing the detectability of total gravity changes by taking into account effects of correlations amongst the diverse measurement points (e.g., Gehman et al., 2009; Jacob et al., 2009, 2010; Christiansen et al., 2011b; Herckenrath et al., 2012).

Figures 8 depict the temporal evolution of the AMAE (14a), Sobol', AMAγ (14b), and AMAk (14c) indices related to the total change in gravimetry. The general temporal dynamics of the AMAE (Figure 8a) and Sobol' (Figure 8b) indices are essentially similar to those displayed by gravimetric variations at the local scale. Note that the total gravimetric change represents the integral of the local scale changes, thus explaining the observed similarity. Skewness and kurtosis of the detected total gravity changes are essentially influenced by all system parameters throughout the temporal window examined. This suggest that there is a clear potential that global gravity changes data can contribute to the identification of the main system parameters.

Figure 9 depicts the spatial distribution of the mean and variance of drawdowns calculated throughout a vertical cross-section (each point being identified by coordinates (*r*, *z*)) at three selected representative times, i.e., t = 100 s (early time behavior), 4 hours (intermediate time, where the effects of specific storage decrease), and 7 days (pseudo-steady state). Since we verified that the spatial distributions of the AMAE and Sobol' indices provide very similar information (not shown), our illustrations focus solely on the Sobol' indices (Figure 9). We also observed that the behavior of parameter a_{cD} (which is associated with the water retention curve) is very similar to the behavior of parameter a_{kD} (which is involved in the relative conductivity model). Therefore, we do not represent the behavior of a_{cD} in the following plots. Note that the quality of the graphical depictions depends on the spacing of the points at which the analytical solution has been determined. A finer grid will provide smoother maps, requiring an increased computer time (see Section 3).

Figure 9 suggests that the mean drawdown is less than 1 m even close to the well after 100 s of pumping, its associated variance being mainly due to the uncertainty of the specific storage S_S. The contribution of S_S to the variance tends to increase at locations close to the well.

Results after 4 hours show that the drawdown is equal to 4 m on average around the pumping well. The sensitivity of S_S is significantly decreased at this time, as compared to early withdrawal times. Otherwise, we can see that the value of the total Sobol' indices of S_Y, K_D, and a_{kD} are enhanced with respect to the corresponding early time results. The spatial distribution of the Sobol' indices related to the parameters linked to hydraulic conductivity (

K_D and a_{kD}) is very different than that associated with the remaining parameters. The indices are higher close to the well for K_D and higher far from the well for a_{kD}.

On day 7 from the beginning of pumping, the mean of the drawdown varies between 4 and 6 m, the highest drawdown being more than 6 m near the well. At this time, the variance of the drawdowns is controlled mainly by the contributions of the parameters related to unsaturated flow (i.e., S_Y, a_{kD}, and a_{cD}) and by the factor of anisotropy (K_D).

The contribution of the parameters involved in the unsaturated flow (water retention and relative conductivity) to the drawdown variance increases with time. This implies that the uncertainty of the drawdowns for long times depends on the hydrodynamic behavior of the unsaturated zone. These parameters do not affect drawdowns uncertainty for short times, when the amount of pumped water is mainly linked to the specific storage (see sensitivity of S_S at time equal to 100 s) and to hydraulic parameters of the saturated zone at the intermediate times (see sensitivity of K_D at time 4 hours).

The distribution of the mean and variance of the global gravity changes and the related Sobol' indices are depicted in Figure 10. The hydrogeological system parameters that do not contribute to the variance significantly and are not included in the figure. Volumetric parameters (i.e., specific storage and specific yield) and the parameter a_{cD} appearing in (7) are the only contributors to the gravimetric changes variance. Gravity changes at t = 100 s are very small. At 4 hours and 7 days after the beginning of the pumping, the spatial distributions of the gravity changes indicate that only the changes of the mass of water within a radius of about 15 m and over a depth less than 15 m contribute to the gravimetric variations (Figure 10).

Close to the surface, gravimetric variations are essentially controlled by the specific yield and a_{cD}. The sensitivity of the specific storage and specific yield respectively decreases and increases with depth (Figure 10). At some depths (such as, e.g., at point A, as illustrated in Section 4.2.1), these variations are controlled by the effects of both specific storage and specific yield. The sensitivity of the specific storage decreases with time, similar to its impact on the drawdown. Otherwise, sensitivity of the specific yield slightly increases with time.

5. Conclusions

Our work is focused on the assessment of the strength of the relative contribution of typically uncertain parameters governing flow in variably saturated porous media to gravity changes that can be recorded during pumping tests in unconfined aquifers. We model drawdown by way of the fully three-dimensional analytical solution of Mishra and Neuman (2011), which explicitly takes into account flow processes across the unsaturated and saturated zones and storage effects in a finite radius pumping well. Gravimetric variations induced by the change of hydraulic head due to pumping and detected by a gravimeter installed at the pumping well location are quantified via the formulations of Telford et al. (1990) and Leirião et al. (2009). We base our study on a Global Sensitivity Analysis approach and quantify the effects of the uncertain model parameters on four statistical moments of gravimetric variations associated with pumping. Our work leads to the following major conclusions.

1. The strength of the relative contribution of saturated and unsaturated zone parameters to the mean and variance of local drawdown, effective saturation, as well as local and global gravimetric variations markedly varies over time. This behavior is quantified through (*a*) recently developed indices (Dell'Oca et al., 2017) quantifying the relative contribution of each uncertain model parameter to the (ensemble) mean, skewness and kurtosis of the model output, and (*b*) the classical Sobol' indices, derived from a decomposition of variance. Our result document that the uncertainty associated with a

given model parameter can impact the first four (statistical) moments of the variables analyzed in a different way, as expressed through the set of sensitivity indices we consider.

2. The mean and the variance of the changes in gravity are mainly controlled by the uncertainty associated with specific yield, the parameter of the water retention curve a_{cD} (7), and aquifer specific storage. All uncertain system parameters considered in the analysis are influential to the skewness and kurtosis, respectively expressing the degree of asymmetry and tailedness of the probability density function of gravity changes.
3. The mean and the variance of drawdown are sensitive to specific storage solely at the beginning of the pumping test. The most significant contributions to the mean and variance of drawdown at late pumping times are due to the uncertainty related to the parameters driving flow in the unsaturated zone.
4. Sample probability density functions of total gravity changes can be interpreted through Exponential distributions (see Figure 7). Our results suggest that in some regions of the parameter space gravity changes at late time (i.e., 7 days) can be significant and larger than about 3 μGal, a value corresponding approximately to reported modern gravimeter accuracy.
5. The results of our Global Sensitivity Analysis suggest that, under the assumptions associated with the analytical model considered, gravimetric data tend to provide limited contribution for the estimation of hydraulic conductivity in the saturated or unsaturated regions, the variance and the mean of drawdowns being more sensitive to these model parameters. Otherwise, gravity data might contribute to infer estimates of aquifer storage terms and water retention curve parameters. From a practical point of view, coupling gravimetric and drawdown measurements during a pumping test have a

high potential to yield improved estimates of saturated and unsaturated regions flow parameters. A natural extension of the study is also related to the assessment of the way the use of the comprehensive set of sensitivity metrics can complement methods based solely on the Sobol' indices (e.g., Ciriello et al., 2013b, 2015) for a design of experiments targeted to prioritize data acquisition for the characterization of specific features of the probability distribution of a desired variable.

References

Alnes, H., Eiken, O., & Stenvold, T. (2008), Monitoring gas production and CO2 injection at the Sleipner field using time-lapse gravimetry, *GEOPHYSICS*, *73*(6), WA155-WA161, doi:10.1190/1.2991119.

Andersen, O. B., & Hinderer, J. (2005), Global inter-annual gravity changes from GRACE: Early results, *Geophys. Res. Lett.*, *32*(1), L01402, doi:10.1029/2004GL020948.

Andersen, O. B., Seneviratne, S. I., Hinderer, J., & Viterbo, P. (2005), GRACE-derived terrestrial water storage depletion associated with the 2003 European heat wave, *Geophys. Res. Lett.*, *32*(18), L18405, doi:10.1029/2005GL023574.

Archer, G. E. B., Saltelli, A., & Sobol, I. M. (1997), Sensitivity measures, ANOVA like techniques and the use of bootstrap, J. *Stat. Comput. Simul*., 58, 99-120

B. Feil, S. K. (2009), Comparison of Monte Carlo and Quasi Monte Carlo Sampling Methods in High Dimensional Model Representation, 12–17, doi:10.1109/SIMUL.2009.34.

Barlow, P. M., & Moench, A. F. (1999), WTAQ—A computer program for calculating drawdowns and estimating hydraulic properties for confined and water-table aquifers, *U.S. Geol. Surv. Water Resour. Invest*. Rep. 99- 4225, 36 pp.

Bevan, M. J., Endres, A. L., Rudolph, D. L., & Parkin, G. (2003), The non-invasive characterization of pumping-induced dewatering using ground penetrating radar, *J. Hydrol.*, *281*(1), 55–69, doi:10.1016/S0022-1694(03)00200-2.

Blainey, J. B., Ferré, T. P. A., & Cordova, J. T. (2007), Assessing the likely value of gravity and drawdown measurements to constrain estimates of hydraulic conductivity and specific yield during unconfined aquifer testing, *Water Resour. Res.*, *43*(12), W12408, doi:10.1029/2006WR005678.

Blatman, G., & Sudret, B. (2010a), An adaptive algorithm to build up sparse polynomial chaos expansions for stochastic finite element analysis, *Probabilistic Eng. Mech.*, *25*(2), 183–197, doi:10.1016/j.probengmech.2009.10.003.

Blatman, G., & Sudret, B. (2010b), Efficient computation of global sensitivity indices using sparse polynomial chaos expansions, *Reliab. Eng. Syst. Saf.*, *95*(11), 1216–1229, doi:10.1016/j.ress.2010.06.015.

Blatman, G., & Sudret, B. (2011), Adaptive sparse polynomial chaos expansion based on least angle regression, *J. Comput. Phys.*, *230*(6), 2345–2367, doi:10.1016/j.jcp.2010.12.021.

Chang, P.-Y., Chang, L.-C., Hsu, S.-Y., Tsai, J.-P., & Chen, W.-F. (2017.), Estimating the hydrogeological parameters of an unconfined aquifer with the time-lapse resistivity-imaging method during pumping tests: Case studies at the Pengtsuo and Dajou sites, Taiwan, *J. Appl. Geophys.*, doi:10.1016/j.jappgeo.2017.06.014.

Christiansen, L., Binning, P. J., Rosbjerg, D., Andersen, O. B., & Bauer-Gottwein, P. (2011a), Using time-lapse gravity for groundwater model calibration: An application to alluvial aquifer storage, *Water Resour. Res.*,47, W06503, doi:10.1029/2010WR009859.

Christiansen, L., Lund, S., Andersen, O. B., Binning, P. J., Rosbjerg, D., & Bauer-Gottwein, P. (2011b), Measuring gravity change caused by water storage variations: Performance assessment under controlled conditions,*J. Hydrol.*, 402(1–2), 60–70.

Ciriello, V., Di Federico, V., Riva, M., Cadini, F., De Sanctis, J., Zio, E., & Guadagnini, A. (2013a), Polynomial Chaos Expansion for Global Sensitivity Analysis applied to a model of radionuclide migration in a randomly heterogeneous aquifer, *Stoch. Environ. Res. Risk Assess.*, 27, 945-954, doi:10.1007/s00477-012-0616-7.

Ciriello, V., Guadagnini, A., Di Federico, V., Edery, Y., & Berkowitz, B. (2013b), Comparative analysis of formulations for conservative transport in porous media through sensitivity-based parameter calibration, *Water Resour. Res.*, 49, 5206-5220, doi:10.1002/wrcr.20395.

Ciriello, V., Edery, Y., Guadagnini, A., & Berkowitz, B. (2015), Multimodel framework for characterization of transport in porous media, *Water Resour. Res.*, 51(5), 3384-3402, doi:10.1002/2015WR017047.

Crestaux, T., Le Maître, O., & Martinez, J.-M. (2009), Polynomial chaos expansion for sensitivity analysis, *Reliab. Eng. Syst. Saf.*, *94*(7), 1161–1172, doi:10.1016/j.ress.2008.10.008.

Damiata, B. N., & Lee, T.-C. (2006), Simulated gravitational response to hydraulic testing of unconfined aquifers, *J. Hydrol.*, *318*(1–4), 348–359, doi:10.1016/j.jhydrol.2005.06.024.

Delay, F., Ackerer, P., Belfort, B., & Guadagnini, A. (2012), On the emergence of reciprocity gaps during interference pumping tests in unconfined aquifers, *Adv. Water Resour.*, *46*, 11–19, doi:10.1016/j.advwatres.2012.06.002.

Dell’Oca, A., Riva, M., & Guadagnini, A. (2017), Moment-based Metrics for Global Sensitivity Analysis of Hydrological Systems, *Hydrol. Earth Syst. Sci.*, 21, 6219-6234, doi:10.5194/hess-21-6219-2017

Eiken, O., Stenvold, T., Zumberge, M., Alnes, H., & Sasagawa, G. (2008), Gravimetric monitoring of gas production from the Troll field, *GEOPHYSICS*, *73*(6), WA149-WA154, doi:10.1190/1.2978166.

Fajraoui, N. (2014), Analyse de sensibilité globale et polynômes de chaos pour l’estimation des paramètres : application aux transferts en milieu poreux, Thèse Doctorat, Université de Strasbourg, 21 January.

Fajraoui, N., Ramasomanana, F., Younes, A., Mara, T. A., Ackerer, P., & Guadagnini, A. (2011), Use of global sensitivity analysis and polynomial chaos expansion for interpretation of nonreactive transport experiments in laboratory-scale porous media, *Water Resour. Res.*, *47*(2), W02521, doi:10.1029/2010WR009639.

Fajraoui, N., Mara, T. A., Younes, A., & Bouhlila, R. (2012), Reactive Transport Parameter Estimation and Global Sensitivity Analysis Using Sparse Polynomial Chaos

Expansion, *Water. Air. Soil Pollut.*, *223*(7), 4183–4197, doi:10.1007/s11270-012-1183-8.

Formaggia, L., Guadagnini, A., Imperiali, I., Lever, V., Porta, G., Riva, M., Scotti, A., & Tamellini, L. (2012), Global sensitivity analysis through polynomial chaos expansion of a basin-scale geochemical compaction model, *Comput. Geosci.*, *17*(1), 25–42, doi:10.1007/s10596-012-9311-5.

Garcia-Cabrejo, O., & Valocchi, A. (2014), Global Sensitivity Analysis for multivariate output using Polynomial Chaos Expansion, *Reliab. Eng. Syst. Saf.*, *126*, 25–36, doi:10.1016/j.ress.2014.01.005.

Gardner, W. R. (1958), Some steady state solutions of the unsaturated moisture flow equation with application to evaporation from water table, *Soil Sci.*, 85, 244-249,, doi:10.1097/00010694-195804000-00006.

Gehman, C. L., Harry, D. L., Sanford, W. E., Stednick, J. D., & Beckman, N. A. (2009), Estimating specific yield and storage change in an unconfined aquifer using temporal gravity surveys, *Water Resour. Res.*, *45*(4), W00D21, doi:10.1029/2007WR006096.

González-Quirós, A. & Fernández-Álvarez, J.P. (2017), Forward Coupled Modeling and Assessment of Gravity Anomalies Caused by Pumping Tests in Unconfined Aquifers Under UnsteadyState Conditions, *Math Geosci* 49: 603. https://doi.org/10.1007/s11004-016-9634-1

Hantush, M. S. (1964), Drawdown around Wells of variable discharge, *J. Geophys. Res.*, *69*(20), 4221–4235, doi:10.1029/JZ069i020p04221.

Herckenrath, D., Auken, E., Christiansen, L., Behroozmand, A. A., & Bauer-Gottwein, P. (2012), Coupled hydrogeophysical inversion using time-lapse magnetic resonance sounding and time-lapse gravity data for hydraulic aquifer testing: Will it work in practice?, *Water Resour. Res.*, *48*(1), W01539, doi:10.1029/2011WR010411.

Hinderer, J. et al. (2009), The GHYRAF (Gravity and Hydrology in Africa) experiment : description and first results, *J. Geodyn.*, *48*(3–5), 172–181, doi:10.1016/j.jog.2009.09.014.

Hinderer, J., Calvo, M., Abdelfettah, Y., Hector, B., Riccardi, U., Ferhat, G., & Bernard, J.-D. (2015), Monitoring of a geothermal reservoir by hybrid gravimetry; feasibility study applied to the Soultz-sous-Forêts and Rittershoffen sites in the Rhine graben, *Geotherm. Energy*, *3*, 16, doi:10.1186/s40517-015-0035-3.

Hunt, T., & Bowyer, D. (2007), Reinjection and gravity changes at Rotokawa geothermal field, New Zealand, *Geothermics*, *36*(5), 421–435, doi:10.1016/j.geothermics.2007.07.004.

Hunt, T. M. (1977), Recharge of water in Wairakei Geothermal Field determined from repeat gravity measurements, *N. Z. J. Geol. Geophys.*, *20*(2), 303–317, doi:10.1080/00288306.1977.10420709.

Hunt, T. M., & Graham, D. J. (2009), Gravity changes in the Tauhara sector of the Wairakei–Tauhara geothermal field, New Zealand, *Geothermics*, *38*(1), 108–116, doi:10.1016/j.geothermics.2008.12.003.

Jacob, T., Bayer, R., Chery, J., Jourde, H., Moigne, N. L., Boy, J.-P., Hinderer, J., Luck, B., & Brunet, P. (2008a), Absolute gravity monitoring of water storage variation in a karst aquifer on the larzac plateau (Southern France), *J. Hydrol.*, *359*(1–2), 105–117, doi:10.1016/j.jhydrol.2008.06.020.

Jacob, T., Bayer, R., Chery, J., Jourde, H., Moigne, N. L., Boy, J.-P., Hinderer, J., Luck, B., & Brunet, P. (2008b), Absolute gravity monitoring of water storage variation in a karst aquifer on the larzac plateau (Southern France), *J. Hydrol.*, *359*(1–2), 105–117, doi:10.1016/j.jhydrol.2008.06.020.

Jacob, T., Chery, J., Bayer, R., Le Moigne, N., Boy, J.-P., Vernant, P., & Boudin, F. (2009), Time-lapse surface to depth gravity measurements on a karst system reveal the dominant role of the epikarst as a water storage entity, *Geophys. J. Int.*, *177*(2), 347–360, doi:10.1111/j.1365-246X.2009.04118.x.

Jacob, T., Bayer, R., Chery, J., & Le Moigne, N. (2010), Time-lapse microgravity surveys reveal water storage heterogeneity of a karst aquifer, *J. Geophys. Res. Solid Earth*, *115*(B6), B06402, doi:10.1029/2009JB006616.

Kabirzadeh, H., Kim, J. W., & Sideris, M. G. (2017), Micro-gravimetric monitoring of geological CO2 reservoirs, *Int. J. Greenh. Gas Control*, *56*, 187–193, doi:10.1016/j.ijggc.2016.11.028.

Katterbauer, K., Arango, S., Sun, S., & Hoteit, I. (2017), Integrating gravimetric and interferometric synthetic aperture radar data for enhancing reservoir history matching of carbonate gas and volatile oil reservoirs, *Geophys. Prospect.*, *65*(1), 337–364, doi:10.1111/1365-2478.12371.

Leirião, S., He, X., Christiansen, L., Andersen, O. B., & Bauer-Gottwein, P. (2009), Calculation of the temporal gravity variation from spatially variable water storage change in soils and aquifers, *J. Hydrol.*, *365*(3–4), 302–309, doi:10.1016/j.jhydrol.2008.11.040.

Merlet, S., Kopaev, A., Diament, M., Geneves, G., Landragin, A., & Dos Santos, F. P. (2008), Microgravity investigations for the LNE watt balance project, *Metrologia* 45(3), 265-274.

Mishra, P. K., & Neuman, S. P. (2010), Improved forward and inverse analyses of saturated-unsaturated flow toward a well in a compressible unconfined aquifer, *Water Resour. Res.*, *46*(7), W07508, doi:10.1029/2009WR008899.

Mishra, P. K., & Neuman, S. P. (2011), Saturated-unsaturated flow to a well with storage in a compressible unconfined aquifer, *Water Resour. Res.*, *47*(5), W05553, doi:10.1029/2010WR010177.

Moench, A. F. (1996), Flow to a Well in a Water-Table Aquifer: An Improved Laplace Transform Solution, *Ground Water*, *34*(4), 593–596, doi:10.1111/j.1745-6584.1996.tb02045.x.

Moench, A. F. (1997a), Flow to a well of finite diameter in a homogeneous, anisotropic water table aquifer, *Water Resour. Res.*, *33*(6), 1397–1407, doi:10.1029/97WR00651.

Moench, A. F. (1997b), Flow to a well of finite diameter in a homogeneous, anisotropic water table aquifer, *Water Resour. Res.*, *33*(6), 1397–1407, doi:10.1029/97WR00651.

Moench, A. F. (2008), Analytical and numerical analyses of an unconfined aquifer test considering unsaturated zone characteristics, *Water Resour. Res.*, *44*(6), W06409, doi:10.1029/2006WR005736.

Montgomery, E. L. (1971), Determination of coefficient of storage by use of gravity measurements., . Ph.D. Thesis, University of Arizona, Tucson.

Naujoks, M., Kroner, C., Weise, A., Jahr, T., Krause, P., & Eisner, S. (2010), Evaluating local hydrological modelling by temporal gravity observations and a gravimetric three-dimensional model, *Geophys. J. Int.*, *182*(1), 233–249, doi:10.1111/j.1365-246X.2010.04615.x.

Neuman, S. P. (1972), Theory of flow in unconfined aquifers considering delayed response of the water table, *Water Resour. Res.*, *8*(4), 1031–1045, doi:10.1029/WR008i004p01031.

Neuman, S. P. (1974), Effect of partial penetration on flow in unconfined aquifers considering delayed gravity response, *Water Resour. Res.*, *10*(2), 303–312, doi:10.1029/WR010i002p00303.

Pfeffer, J., Boucher, M., Hinderer, J., Favreau, G., Boy, J.-P., de Linage, C., Cappelaere, B., Luck, B., Oi, M., & Le Moigne, N. (2011), Local and global hydrological contributions to time-variable gravity in Southwest Niger, *Geophys. J. Int.*, *184*(2), 661–672, doi:10.1111/j.1365-246X.2010.04894.x.

Pianosi, F., & Wagener, T. (2015), A simple and efficient method for global sensitivity analysis based on cumulative distribution functions, *Environ. Model. Softw.*, *67*, 1–11, doi:10.1016/j.envsoft.2015.01.004.

Pool, D. R. (2005), Variations in climate and ephemeral channel recharge in southeastern Arizona, United States, *Water Resour. Res.*, *41*(11), W11403, doi:10.1029/2004WR003255.

Pool, D. R. (2008), The utility of gravity and water-level monitoring at alluvial aquifer wells in southern Arizona, *Geophysics*, *73*(6), doi:10.1190/1.2978166.

Pool, D. R., & Eychaner, J. H. (1995), Measurements of aquifer-storage change and specific yield using gravity surveys, *Groundwater*, *33*(3), 425432, doi:10.1111/j.1745-6584.1995.tb00299.x.

Raghavan, R. (2004), A review of applications to constrain pumping test responses to improve on geological description and uncertainty, *Rev. Geophys.*, *42*(4), RG4001, doi:10.1029/2003RG000142.

Razavi, S., & Gupta, H. V. (2015), What do we mean by sensitivity analysis? The need for comprehensive characterization of "global" sensitivity in Earth and Environmental systems models, *Water Resour. Res.*, *51*(5), 3070–3092, doi:10.1002/2014WR016527.

Richards, L. A. (1931), Capillary conduction of liquids through porous medium, *J. Appl. Phys.*, *1*(5), 318–333, doi:10.1063/1.1745010.

Rizzo, E., Suski, B., Revil, A., Straface, S., & Troisi, S. (2004), Self-potential signals associated with pumping tests experiments, *J. Geophys. Res. Solid Earth*, *109*(B10), B10203, doi:10.1029/2004JB003049.

Sarrazin, F., Pianosi, F., & Wagener, T. (2016), Global Sensitivity Analysis of environmental models: Convergence and validation, *Environ. Model. Softw.*, *79*, 135–152, doi:10.1016/j.envsoft.2016.02.005.

Sobol, I. M. (1993), Sensitivity estimates for nonlinear mathematical models, *Math. Model. Comput.*, 1, 407–414.

Sofyan, Y., Kamah, Y., Nishijima, J., Fujimitsu, Y., Ehara, S., Fukuda, Y., & Taniguchi, M. (2011), Mass variation in outcome to high production activity in Kamojang Geothermal Field, Indonesia: A reservoir monitoring with relative and absolute gravimetry, *Earth Planets Space*, *63*(11), 1157–1167, doi:10.5047/eps.2011.07.005.

Straface, S., Fallico, C., Troisi, S., Rizzo, E., & Revil, A. (2007), An inverse procedure to estimate transmissivity from heads and SP signals, *Ground Water*, *45*(4), 420–428, doi:10.1111/j.1745-6584.2007.00310.x.

Sudret, B. (2008), Global sensitivity analysis using polynomial chaos expansions, *Reliab. Eng. Syst. Saf.*, *93*(7), 964–979, doi:10.1016/j.ress.2007.04.002.

Sudret, B., & Mai, C. V. (2015), Computing derivative-based global sensitivity measures using polynomial chaos expansions, *Reliab. Eng. Syst. Saf.*, *134*, 241–250, doi:10.1016/j.ress.2014.07.009.

Tapley, B. D., S. Bettadpur, Watkins, M., & Reigber, C. (2004), The gravity recovery and climate experiment: Mission overview and early results, *Geophys. Res. Lett.*, *31*(9), L09607, doi:10.1029/2004GL019920.

Tartakovsky, G. D., & Neuman, S. P. (2007), Three-dimensional saturated-unsaturated flow with axial symmetry to a partially penetrating well in a compressible unconfined aquifer, *Water Resour. Res.*, *43*(1), W01410, doi:10.1029/2006WR005153.

Telford, W. M., Geldart, L. P., & Sheriff, R. E. (1990), *Applied Geophysics*, Cambridge University Press.

Theis, C. V. (1935), The relation between the lowering of the Piezometric surface and the rate and duration of discharge of a well using ground-water storage, *Eos Trans. Am. Geophys. Union*, *16*(2), 519–524, doi:10.1029/TR016i002p00519.

Wilson, C. R., Scanlon, B., Sharp, J., Longuevergne, L., & Wu, H. (2012), Field Test of the Superconducting Gravimeter as a Hydrologic Sensor, *Ground Water*, 50(3), 442–449, doi:10.1111/j.1745-6584.2011.00864.x.

Xiu, D., & Karniadakis, G. E. (2002), The Wiener-Askey polynomial chaos for stochastic differential equations, *J. Sci. Comput.*, 24(2), 619-644.

Young, W., & Lumley, D. (2015), Feasibility analysis for time-lapse seafloor gravity monitoring of producing gas fields in the Northern Carnarvon Basin, offshore Australia, *GEOPHYSICS*, *80*(2), WA149-WA160, doi:10.1190/geo2014-0264.1.

Table caption

Table1. Ranges of variability of model parameters.

Parameters	**Variability range**
S_S (m^{-1})	(10^{-5} - 10^{-3})
S_Y (-)	(10^{-2} - 0.50)
a_{kD} (-)	(2 - 1000)
a_{cD} (-)	(0.1 - 100)
K_D (-)	(0.05 – 1.0)
L_D (-)	(0.01 - 0.70)

Figure caption

Figure 1. Schematic representation of system geometry.

Figure 2. Temporal evolution of the mean (continuous curve) (*a*) drawdown and (*b*) effective saturation calculated within a volume centered at the initial position of the interface between the saturated and the unsaturated zones. The width of the shaded area corresponds to one standard deviation.

Figure 3. Temporal evolution of the mean (continuous curve) gravity changes computed between the initial (undisturbed) condition and time *t* within the same volume considered in Figure 2. The width of the shaded area corresponds to two standard deviations.

Figure 4. Contribution of the uncertainty of each model parameter to (*a*) the mean (AMAE Indices) and to (*b*) the variance (Sobol' indices) of drawdown.

Figure 5. Contribution of the uncertainty of each model parameter to (*a*) the mean (AMAE Indices) and to (*b*) the variance (Sobol' indices) of effective saturation.

Figure 6. Contribution of the uncertainty of each model parameter to (*a*) the mean (AMAE Indices) and to (*b*) the variance (Sobol' indices) of gravity changes.

Figure 7. (*a*) Temporal evolution of the mean gravity change (continuous curve) over the whole domain (the width of the shaded area corresponds to two standard deviations) and (*b*) probability density functions for three selected times

Figure 8. Contribution of the uncertainty of each model parameter to (*a*) the mean (AMAE Index), to (*b*) the variance (Sobol' indices), to (*c*) the skewness (AMAγ Index) and to (*d*) the kurtosis (AMAk Index) of gravity changes over the whole domain

Figure 9. Spatial distribution of the mean and variance of drawdowns and of total Sobol' indices associated with S_S, S_Y, a_{kD}, K_D calculated throughout a vertical cross-section at times t = 100 s, 4 hours, and 7 days.

Figure 10. Spatial distribution of the mean and variance of gravity changes and of total Sobol' indices associated with S_S, S_Y and a_{cD} calculated throughout a vertical cross-section at times t = 100 s, 4 hours, and 7 days.

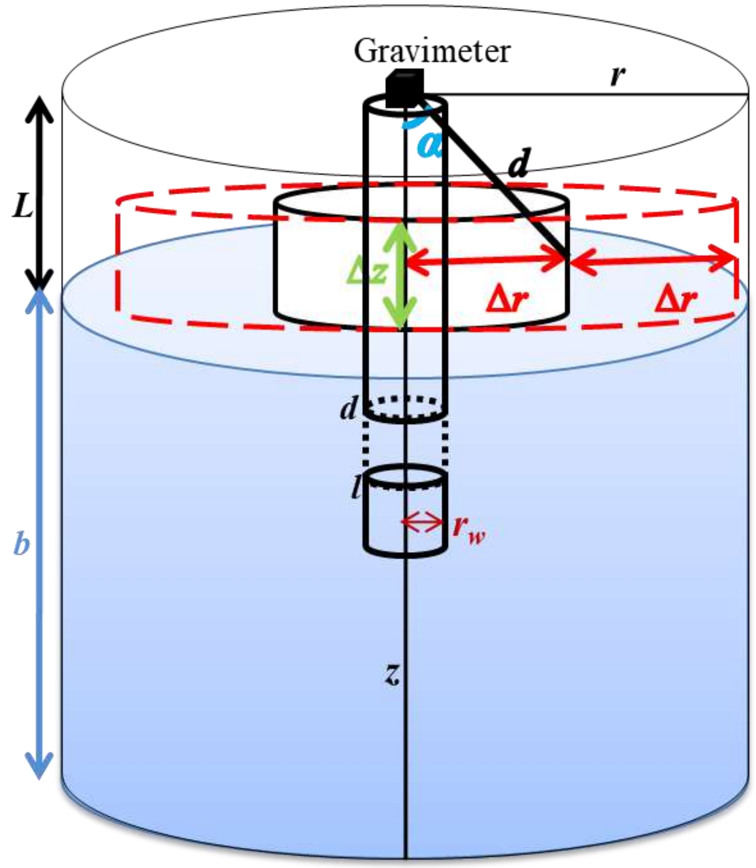

Figure 1: Schematic representation of system geometry

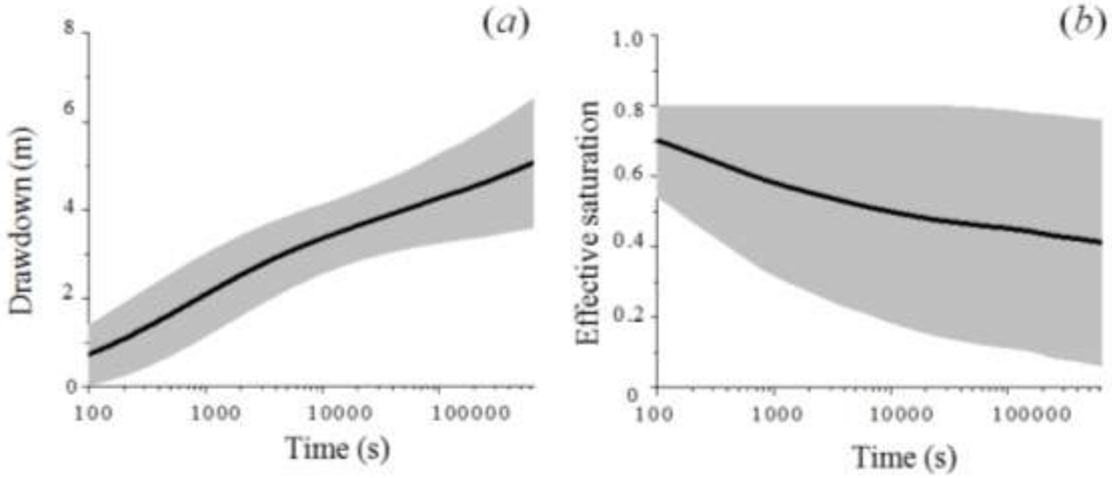

Figure 2 : Temporal evolution of the mean (continuous curve) (*a*) drawdown and (*b*) effective saturation calculated within a volume centered at the initial position of the interface between the saturated and the unsaturated zones. The width of the shaded area corresponds to one standard deviation.

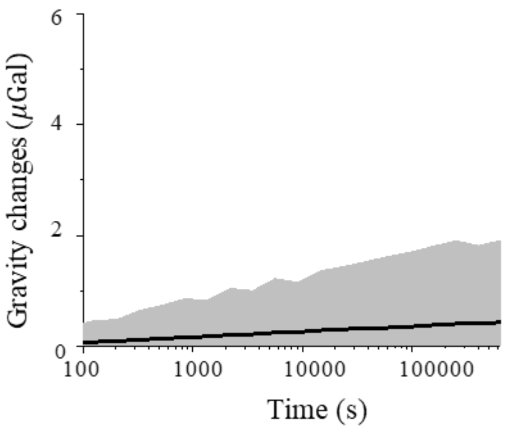

Figure 3: Temporal evolution of the mean (continuous curve) gravity changes computed between the initial (undisturbed) condition and time *t* within the same volume considered in Figure 2. The width of the shaded area corresponds to two standard deviations

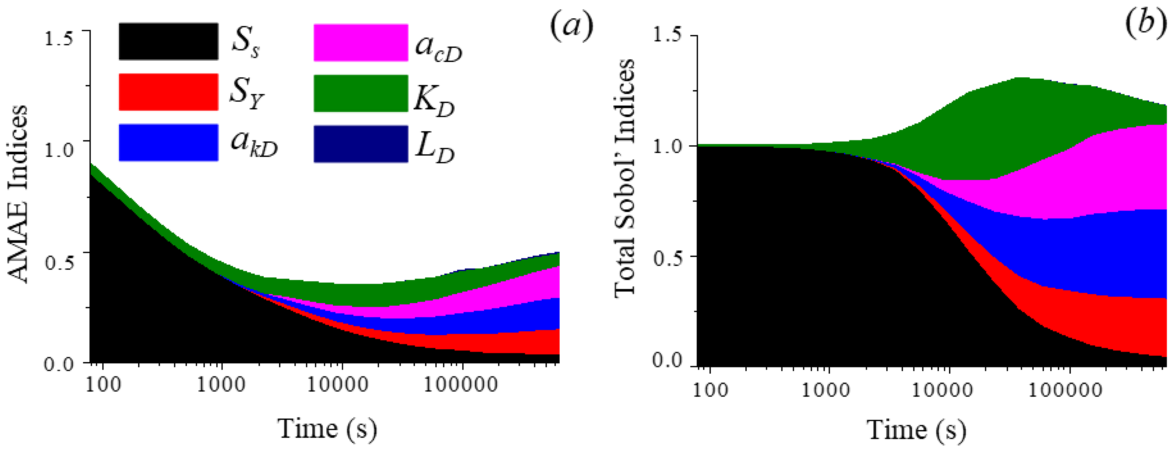

Figure 4: Contribution of the uncertainty of each model parameter to (*a*) the mean (AMAE Indices) and to (*b*) the variance (Sobol' indices) of drawdown.

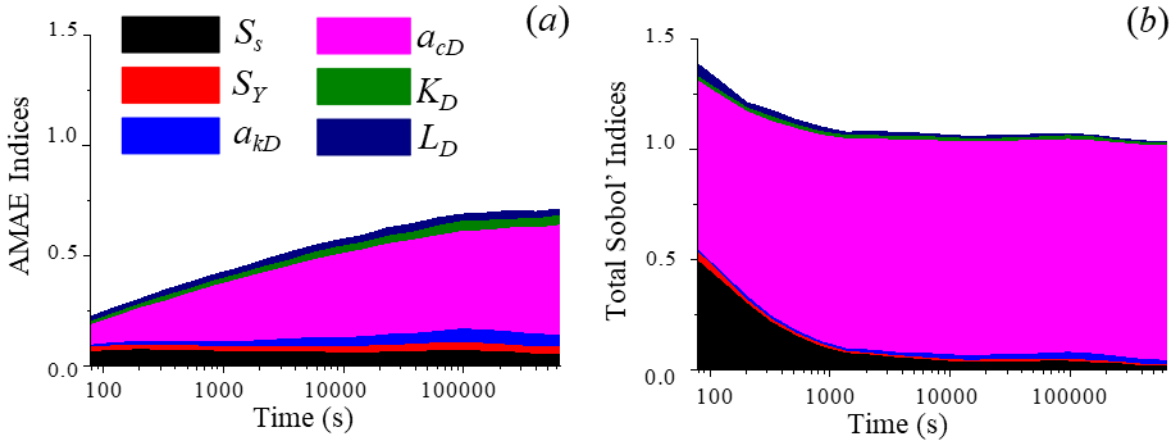

Figure 5: Contribution of the uncertainty of each model parameter to (*a*) the mean (AMAE Indices) and to (*b*) the variance (Sobol' indices) of effective saturation.

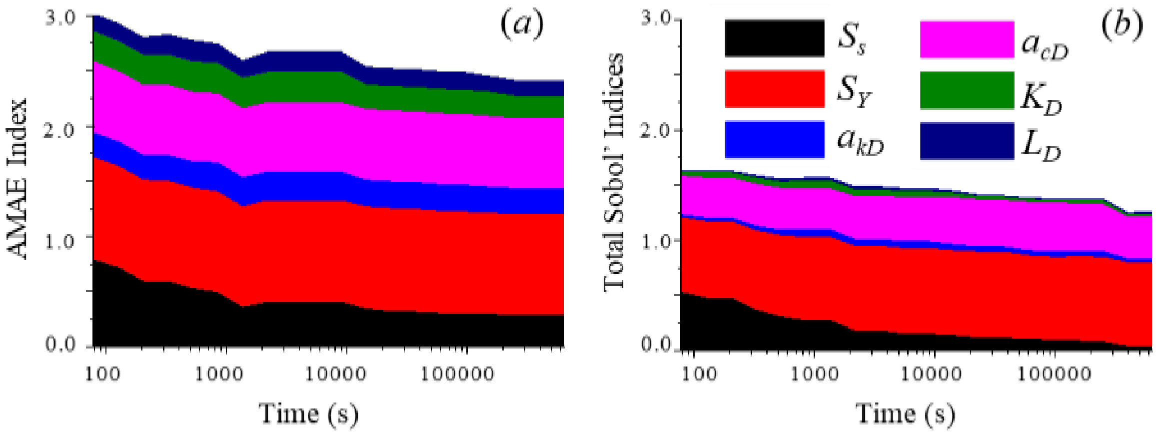

Figure 6: Contribution of the uncertainty of each model parameter to (*a*) the mean (AMAE Indices) and to (*b*) the variance (Sobol' indices) of gravity changes.

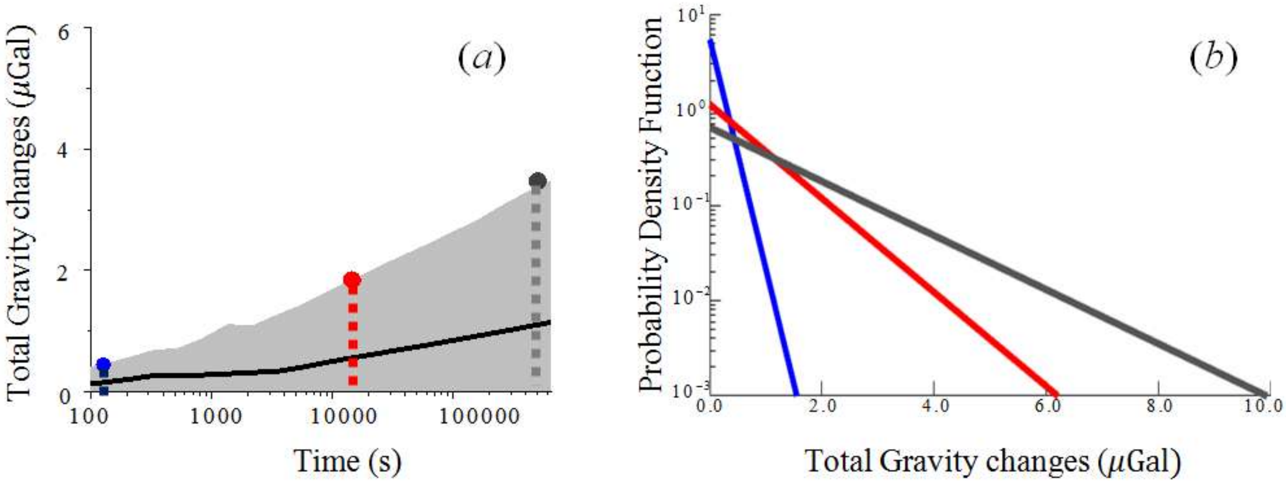

Figure 7: (*a*) Temporal evolution of the mean gravity change (continuous curve) over the whole domain (the width of the shaded area corresponds to two standard deviations) and (*b*) probability density functions for three selected times

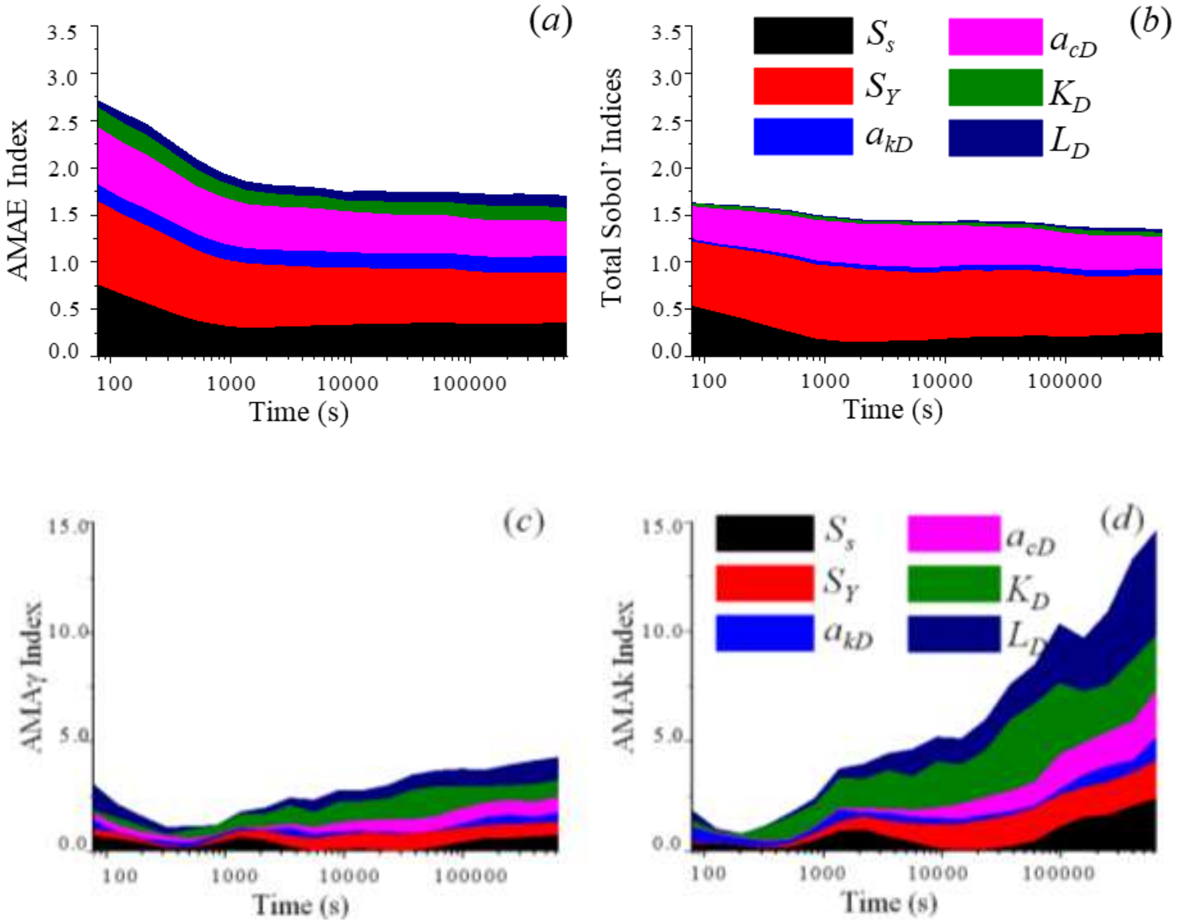

Figure 8: Contribution of the uncertainty of each model parameter to (*a*) the mean (AMAE Index), to (*b*) the variance (Sobol' indices), to (*c*) the skewness (AMAγ Index) and to (*d*) the kurtosis (AMAk Index) of gravity changes over the whole domain

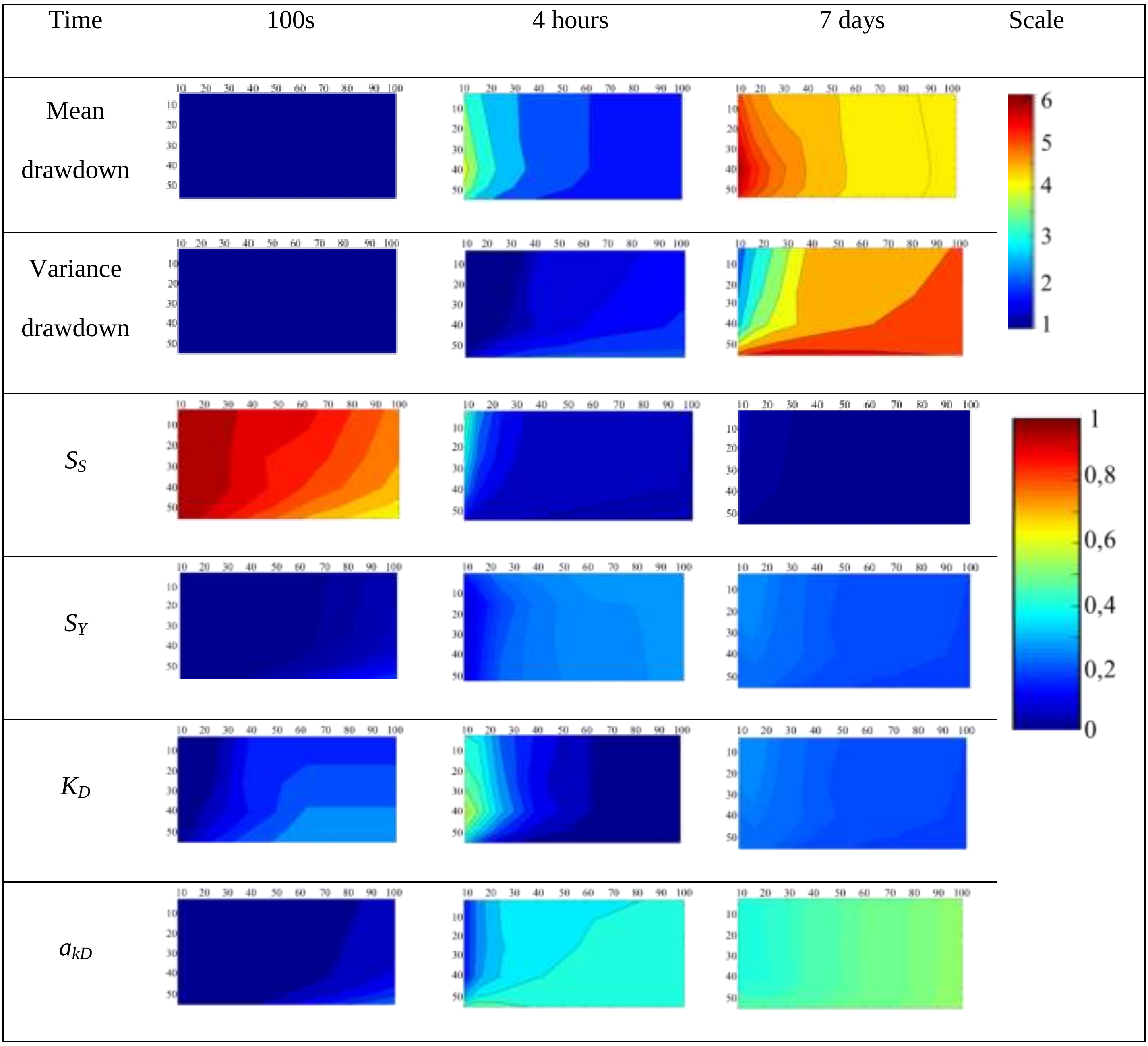

Figure 9 : Spatial distribution of the mean and variance of drawdowns and of total Sobol' indices associated with S_S , S_Y , a_{kD} , K_D calculated throughout a vertical cross-section at times t = 100 s, 4 hours, and 7 days.

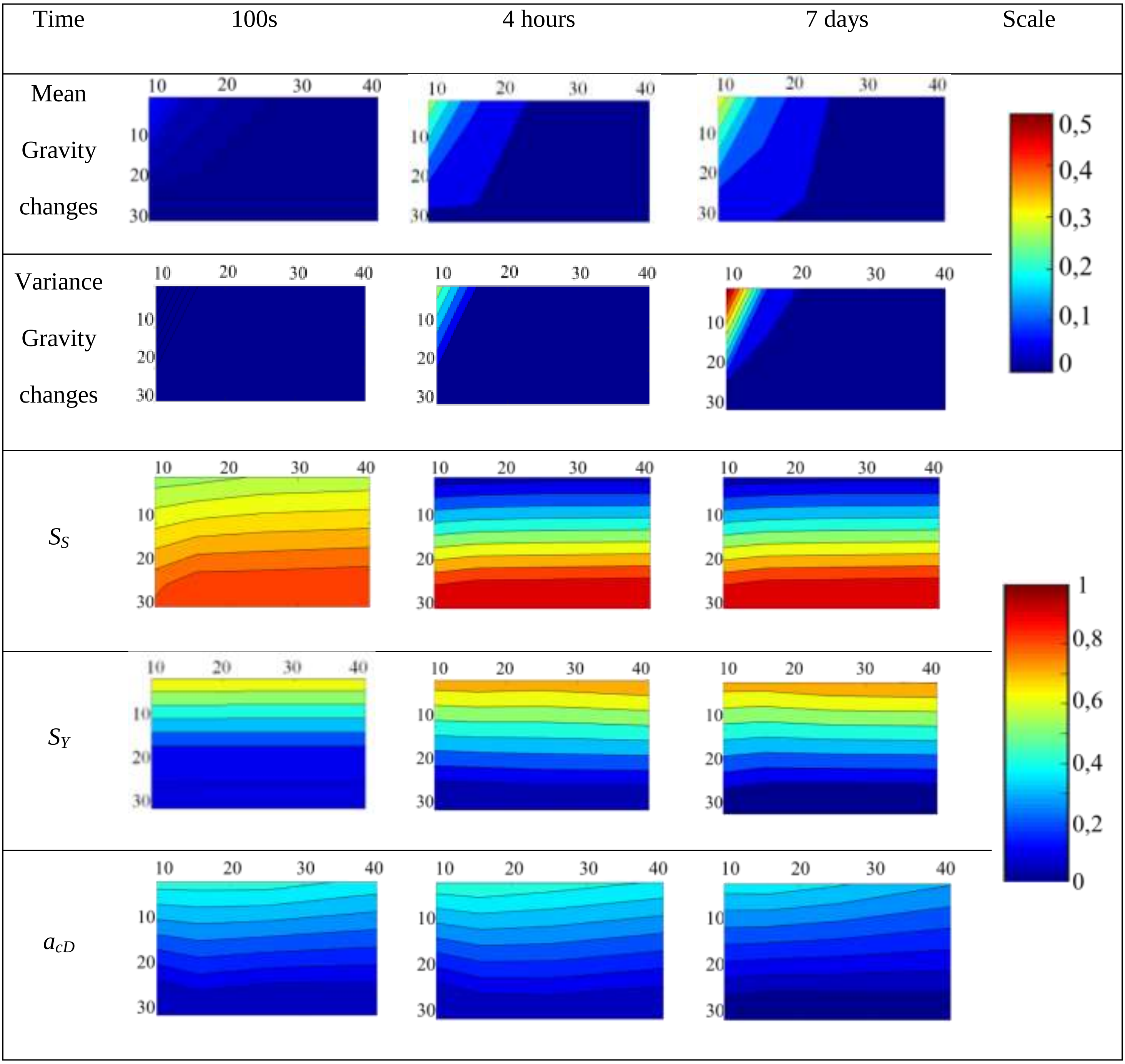

Figure 10 : Spatial distribution of the mean and variance of gravity changes and of total Sobol' indices associated with S_S , S_Y and a_{cD} calculated throughout a vertical cross-section at times t = 100 s, 4 hours, and 7 days.